Journal of Adhesion Science and Technology

Publication details, including instructions for authors and subscription information:
http://www.tandfonline.com/loi/tast20

The Influence of the Fractal Dimension of Rough Surfaces on the Adhesion of Elastic Materials

G. Carbone [a] & E. Pierro [a b]

[a] DIMeG — Politecnico di Bari, v.le Japigia 182, 70126, Bari, Italy

[b] Istituto IOM di Trieste — CNR S.S, 14, Km. 163.5, 34149, Trieste, Italy

Version of record first published: 17 May 2012.

To cite this article: G. Carbone & E. Pierro (2012): The Influence of the Fractal Dimension of Rough Surfaces on the Adhesion of Elastic Materials, Journal of Adhesion Science and Technology, 26:22, 2555-2570

To link to this article: http://dx.doi.org/10.1163/156856111X623140

VSP

Journal of Adhesion Science and Technology 26 (2012) 2555–2570

Journal of ADHESION SCIENCE and TECHNOLOGY
brill.nl/jast

The Influence of the Fractal Dimension of Rough Surfaces on the Adhesion of Elastic Materials

G. Carbone [a,*] **and E. Pierro** [a,b]

[a] DIMeG — Politecnico di Bari, v.le Japigia 182, 70126 Bari, Italy
[b] Istituto IOM di Trieste — CNR S.S. 14, Km. 163.5, 34149 Trieste, Italy

Received on 24 November 2011

Abstract
In this paper we analyse the adhesion between a rubber block and a rigid randomly rough profile. The focus of the investigation is on the influence of the work of adhesion and of the fractal dimension D_f of the rough profile on the contact behaviour. In particular, we analyse how the contact area and the power spectral density of the deformed profile are affected by the two aforementioned quantities. We find that at sufficiently small loads the influence of D_f is negligible. However, the scenario strongly changes at higher loads as D_f strongly affects the number of contact spots. Calculations show that the contact area depends linearly on the work of adhesion, whereas only a negligible influence of the work of adhesion is found on the power spectral density (PSD) of the deformed profile.

Keywords
Contact mechanics, roughness, adhesion, tribology

1. Introduction

Theoretical and experimental research on contact mechanics between rough surfaces is stimulated by the crucial role that this topic plays in a large number of engineering applications, ranging from seals [1–4], boundary and mixed lubrication [5–8], adhesive tapes, MEMS and NEMS, and friction [9–12]. In the last years two main approaches have been developed to study the contact mechanics of an elastic body when it is brought into contact with a rough surface: (i) multiasperity contact theories [13–17] where the contact between the surfaces is modelled as an ensemble of randomly distributed Hertzian contacts between the asperities, and (ii) Persson's theory of contact mechanics [9, 18, 19], where the probability

* To whom correspondence should be addressed. Tel.: +39 080 596 2746; Fax: +39 080 596 2777; e-mail: carbone@poliba.it

 DOI:10.1163/156856111X623140

distribution of the contact pressure is shown to be governed by a diffusive process. Both approaches predict, with some differences, linearity between the contact area and the load in the limiting case of small loads. This has also been confirmed by some numerical and experimental studies [20–26], which have also shown that Persson's theory [9, 27] is able to capture, at least qualitatively, the physical mechanism involved in contact mechanics of rough surfaces. In particular, the predicted linearity between the contact area and the load, which covers the range from 0 to 15–20% of the nominal contact area, is in agreement with the numerical results, as well as the predicted exponent of the power law of the PSD of the interfacial stress distribution. On the other hand, other studies [17, 28] have shown that multiasperity contact theories predict linearity only for very small load values, whereas as the load is increased the theoretical predictions rapidly deviate from the asymptotic linearity. Interestingly, both Persson's theory and multiasperity contact models show that, given the same material properties, the area *vs*. load relation is affected only by the moments of the PSD of the rough surface. However, since many rough surfaces of practical interest are self-affine fractals (e.g., asphalt and concrete roads), one may wonder whether the fractal dimension of the rough surface has also a role in determining the area-load relation.

Since the pioneering investigation of Fuller and Tabor [29], there exist plenty of studies focusing on the adhesion of rough surfaces. These studies mainly use multiasperity models to describe the contact between rough surfaces. Within this framework more recent studies have been carried out to consider also the effect of asperity plastic deformation on the adhesion of rough solids [30]. Unfortunately, multiasperity contact models only approximately describe the contact mechanics between rough surfaces, and, as shown in [28], do not always give satisfactory results, as they neglect interaction and coalescence between asperities. However, multiasperity models have the merit of having clarified the main physical aspects of the contact problem. In this paper we propose a completely different procedure which provides a fully numerically-exact solution of the equation governing the contact between rough surfaces. The methodology, different from finite element model (FEM) [22, 31], is much less expensive from a computational point of view and guarantees to achieve convergent results. FE models have been also used to investigate the adhesion contact in presence of plastic deformation [31], which is neglected in our work because we focus on elastically soft materials, such as poly(dimethylsiloxane) (PDMS), which usually does not exhibit plastic deformation. We concentrate our attention on these type of materials, and investigate the role of the fractal dimension of the rough surface in the area-load and penetration-load relations, by analysing the adhesion contact between a semi-infinite elastic space and periodic self-affine fractal 1D rough surfaces.

Of course, real surfaces present 2D roughness, but there are mainly three reasons for studying 1D rough contacts: (i) first of all one should keep in mind that in order to obtain physically meaningful results, one needs to include in the analysis all the spectral components of the surface roughness (which can cover a range of scales

of about 3–4 orders of magnitude), usually resulting in a strong increase of the computational cost. We observe that this problem is considerably reduced in case of 1D roughness; (ii) secondly we note that rough surfaces, encountered in many practical applications, are often strongly anisotropic mainly as a result of machining and surface treatments (e.g., unidirectional polished surface which presents wear tracks along the polishing direction, although the resulting roughness is not strictly 1D); (iii) thirdly it is possible to generate 1D rough surfaces which are equivalent, from the point of view of contact area *vs*. load relation, to 2D rough surfaces [32, 33].

To deal with the adhesion contact problem we employ a methodology already presented by one of us in [34], based on a pure continuum mechanics approach and belonging to the class of Boundary Element Methods (BEMs) [10, 25]. Our findings suggest that the influence of fractal dimension D_f is negligible only in the range of linearity between the contact area and the applied load, whereas it becomes very significant at higher loads. We also investigate how the number of contacts is affected by the applied load and by D_f. Our calculations show that when D_f is in the range 1–1.1 the number of contacts is relatively small and increases slowly (less than linearly) with the load. In this case the relation between the contact area and load rapidly deviates from linearity. The influence of the Duprè energy of adhesion, also referred to as work of adhesion, both on the contact area and on the PSD of the deformed profiles is studied, as well as the behavior of the probability distribution of local separation (the interfacial voids), which plays a crucial role in many practical applications, as, for example, in determining the fluid leakage in seals, and fluid flow in mixed lubrication.

2. The Numerical Model

In this section we briefly summarise the numerical methodology presented in [34]. We consider a periodic contact where an elastic layer of thickness d is interposed between a flat rigid plate (upper surface) and a periodically rough rigid substrate with wavelength λ (bottom surface) as shown in Fig. 1. We assume that the rough

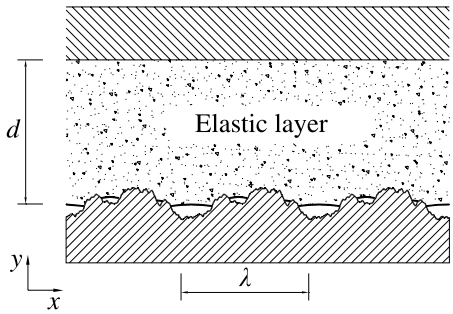

Figure 1. An elastic layer of thickness d in adhesion contact with a rough periodic substrate of wavelength λ.

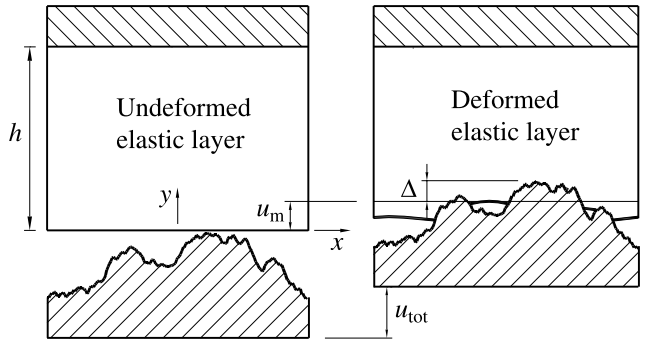

Figure 2. The definition of substrate displacement $u_{\rm tot}$, elastic layer average displacement $u_{\rm m}$ and substrate penetration Δ into the elastic layer.

surface has roughness in only one direction and is smooth in the orthogonal direction. Under these conditions the problem at hand is a periodic plane problem, i.e., the stress, displacement and strain fields depend only on the x and y coordinates and have a periodicity λ. Figure 2 shows the total displacement $u_{\rm tot}$ of the substrate, the average displacement $u_{\rm m}$ of the elastic layer, and the penetration Δ of the rigid substrate into the elastic layer. These three quantities are shown to satisfy the following relation

$$u_{\rm tot} = \Delta + u_{\rm m}. \tag{1}$$

We will focus on the pressure distribution $\sigma(x)$ and interfacial displacement fluctuation $v(x) = u(x) - u_{\rm m}$. In [10] and [34] it has been shown that the unknown pressure distribution in the contact area Ω can be determined by solving the following Fredholm integral equation of the first kind with a logarithmic kernel

$$-\int_{\Omega} \mathcal{G}(x-s)\sigma(s)\,{\rm d}s = [h(x) - h_{\max}] + \Delta; \quad x \in \Omega, \tag{2}$$

where $\Omega = \bigcup_{i=1}^{L}[a_i, b_i]$ is the unknown contact domain. The quantities a_i and b_i are the unknown coordinates of the ith contact patch with $a_i < b_i$ and $i = 1, 2, \ldots, L$, where L is the unknown number of contacts. In equation (2), assuming the elastic layer is infinitely thick (i.e., $d \to +\infty$), the kernel is

$$\mathcal{G}(x) = \frac{2(1-\nu^2)}{\pi E} \log\left[2\left|\sin\left(\frac{kx}{2}\right)\right|\right] \tag{3}$$

and represents the Green function of the semi-infinite elastic body under a periodic loading, i.e., it represents the displacement $v(x) = u(x) - u_{\rm m}$ caused by the application of a Dirac comb with peaks $\delta(x - n\lambda)$ separated by a distance λ. Here E and ν are Young's modulus and Poisson's ratio of the elastic layer. In equation (2) the quantity $h(x)$ represents the height of the rough profile from its mean plane. Since

we are considering a periodic problem, $h(x)$ can be written in terms of a Fourier series

$$h(x) = \sum_{m=1}^{+\infty} h_m \cos(mq_0 x + \phi_m), \tag{4}$$

where the fundamental wavevector $q_0 = 2\pi/\lambda$, m is the wavenumber and ϕ_m is the phase of the mth spectral component, uniformly distributed in the interval $[0, 2\pi[$. Also we have defined in equation (2) the quantity $h_{\max} = \max[h(x)]$, which is the maximum height of the substrate roughness. Once the pressure distribution is known the elastic displacements at the interface can be easily determined through the equations

$$\begin{aligned} v(x) &= -\int_{\Omega} \mathcal{G}(x-s)\sigma(s)\,\mathrm{d}s; \quad x \in \mathrm{D} - \Omega, \\ v(x) &= h(x) - h_{\max} + \Delta; \quad x \in \Omega, \end{aligned} \tag{5}$$

where $\mathrm{D} = [-\lambda/2, \lambda/2]$. Of course for an infinitely thick layer ($d \to +\infty$ as in our case) the average displacement u_{m} is also infinitely large except when the $\nu = 0.5$, but the difference $v(x) = u(x) - u_{\mathrm{m}}$ is always finite [10, 34] and can be interpreted as the additional elastic displacement of the solid due to the presence of roughness at the interfaces. In order to close the system of equations we need an additional condition to determine the yet unknown contact domain Ω. To this end (see also [34]), we first observe that for any penetration Δ, we can calculate the pressure distribution at the interface through equation (2), and the interfacial elastic displacement through equation (5), as functions of the unknown coordinates a_i and b_i of the ith contact area. To calculate the exact values of the quantities a_i and b_i at equilibrium, given isothermal conditions, we need to minimize the interfacial free energy $U_{\mathrm{tot}}(a_1, b_1, \ldots, a_L, b_L, \Delta)$ of the system at fixed penetration Δ.

The interfacial free energy (see [34]) is

$$U_{\mathrm{tot}} = U_{\mathrm{el}} + U_{\mathrm{ad}}, \tag{6}$$

where the interfacial elastic energy U_{el} is [25]

$$U_{\mathrm{el}}(a_1, b_1, \ldots, a_L, b_L, \Delta) = \frac{1}{2}\sum_{i=1}^{L} \int_{a_i}^{b_i} \sigma(x)[h(x) - h_{\max} + \Delta]\,\mathrm{d}x. \tag{7}$$

The adhesion energy is

$$U_{\mathrm{ad}}(a_1, b_1, \ldots, a_L, b_L) = -\gamma \sum_{i=1}^{L} \int_{a_i}^{b_i} \sqrt{1 + [h'(x)]^2}\,\mathrm{d}x, \tag{8}$$

where γ is the work of adhesion. Equations (2), (5), together with the requirement that the interfacial free energy U_{tot} is a (local) minimum at equilibrium, constitute a set of closed equations which allows, for any given penetration Δ, to determine

the coordinates a_i and b_i of each contact spot, the pressure distribution at the interface, and all other thermodynamic quantities. For the numerical implementation the reader is referred to [25, 34]. The numerical simulations have been carried out for self-affine fractal profiles with PSD

$$C_R(q) = C_0 \left(\frac{|q|}{q_0} \right)^{-(2H+1)}, \tag{9}$$

where H is the Hurst exponent of the randomly rough profile. It is related to the fractal dimension $D_f = 2 - H$. We have utilized a periodic profile with Fourier components in the range $q_0 \leqslant q \leqslant q_1$, with $q_1 = Nq_0$. The rough profiles have been numerically generated by means of spectral techniques shown in [25].

3. Results

We assume that the elastic block is a soft perfectly elastic material with elastic modulus $E = 1$ MPa and Poisson's ratio $\nu = 0.5$. For each rough profile (considered as a stochastic process) results have been averaged over 11 different realizations. The profiles have root mean square roughness $\langle h^2 \rangle^{1/2} = 50$ μm. We have used $\lambda = 2\pi/q_0 = 0.01$ m and $q_1 = 10^3 q_0$. The numerical calculations have been carried out for different values of the separation $s = h_{\max} - \Delta$, which is defined as the distance between the mean plane of the deformed surface and the mean plane of the rough surface. In Fig. 3 we show three different shapes of the deformed profile at three different values of the separation: $s = 86$ μm, $s = 38$ μm and $s = 9.6$ μm. The work of adhesion is $\gamma = 0.03$ J/m^2. The rigid rough substrate profile has a fractal dimension $D_f = 1.3$. A detailed analysis of Fig. 3 shows that full contact always occurs between the elastic block and the short wavelength corrugation of the rough rigid profile, independent of the given value of the separation s. As a consequence, one would expect that for large wavevectors q the slope of the PSD

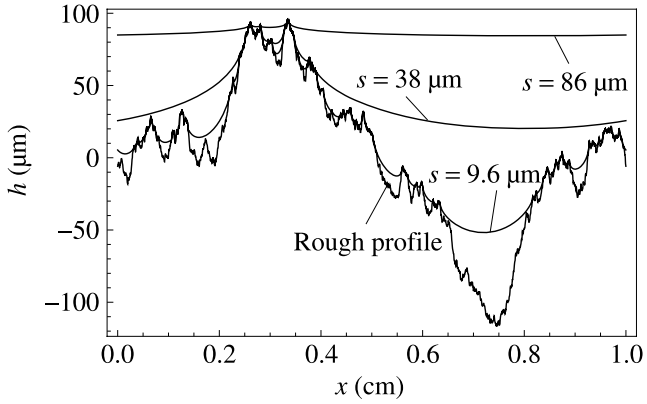

Figure 3. The deformed shapes of the elastic body at three different separations $s = 86$ μm, $s = 38$ μm and $s = 9.6$ μm, and the rough rigid substrate profile.

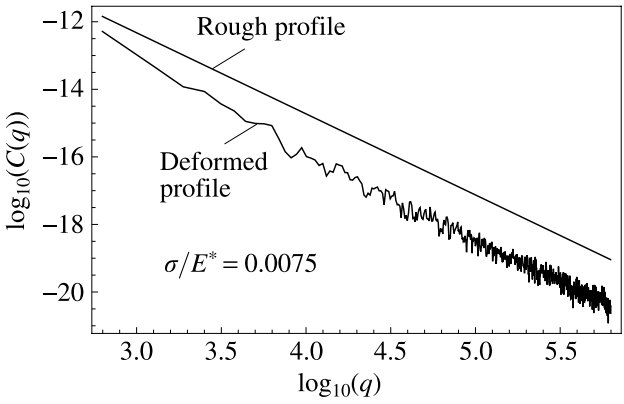

Figure 4. The PSD of the rigid substrate profile with fractal dimension $D_f = 1.3$, compared to the PSD of the deformed shape of the elastic body, obtained for $\gamma = 0.05$ J/m^2, $\sigma/E^* = 0.0075$. $C(q)$ and q are measured in m^3 and m^{-1}, respectively.

of the deformed profile in a log–log diagram should be almost the same as that of the rigid rough profile. This is confirmed in Fig. 4, where the PSD of the rigid substrate profile (fractal dimension $D_f = 1.3$, work of adhesion $\gamma = 0.05$ J/m^2) has been compared to the PSD of the deformed shape of the elastic body. We observe that the curves are almost parallel in the high frequency range. This seems to occur independently of the fractal dimension of the rigid rough profile. To show this, recall first that, as equation (9) shows, in a log–log diagram the PSD of a self-affine rough profile is a straight line with slope $-(2H + 1)$; therefore, if one plots the quantity $(2H + 1)^{-1} \log_{10} C_R(q)$ instead of $C_R(q)$ the PSDs of different profiles are represented by straight lines which are all parallel to each other with slope -1. Figure 5 shows the quantities $(2H + 1)^{-1} \log_{10} C_v(q)$ (where $C_v(q)$ is the PSD of the deformed profile) as a function of the wavevector q for different deformed profiles in contact with self-affine fractals with Hurst exponent $H = 2 - D_f$ equal to 0.7, 0.9 and 1. Results are shown for a dimensionless applied load $\sigma/E^* = 0.0075$, where $E^* = E/(1 - \nu^2)$ is the reduced elastic modulus. At high spatial frequencies, the slope of the curves seems to be exactly the same for all curves and equal to -1. As a reference curve we have plotted the quantity $(2H + 1)^{-1} \log_{10} C_R(q)$ for a rough profile with $H = 1$. This type of behavior is a consequence of the adhesion interactions which, as shown in [18] and [35], cause full contact to occur in the high q-vector range when the Hurst exponent of the surface $H > 0.5$, i.e., $D_f < 1.5$, as indeed happens for the rough profiles we have considered in the numerical simulations. Interestingly Fig. 5 shows that the range of q-vectors where the slope of the curves is -1 extends toward smaller values of q-vector as the Hurst exponent increases. When $H = 1$ we notice that the curve $C_v(q)$ of the deformed profile and the curve $C_R(q)$ of the rough substrate are parallel over the entire q-vector range. We also observe that increasing the fractal dimension reduces the PSD of the deformed profile. This is a consequence of the decrease of contact area caused by

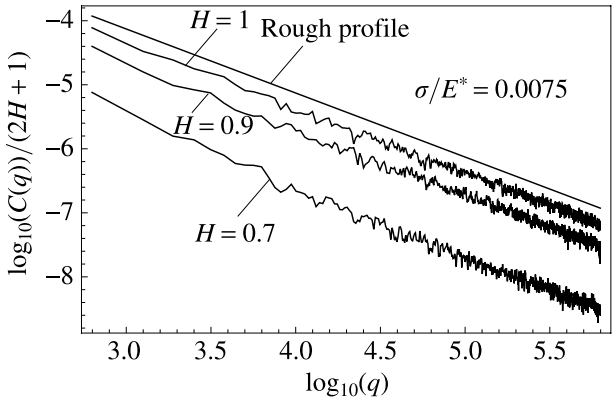

Figure 5. A comparison between the quantities $(2H+1)^{-1}\log_{10} C_v(q)$ obtained as a result of the contact between the elastic layer and three different rough surfaces with Hurst exponents $H = 0.7$, $H = 0.9$ and $H = 1$. The reference curve is the quantity $(2H+1)^{-1}\log_{10} C_R(q)$ for a rough surface with $H = 1$. At large q-vectors, the slope of the curves is -1, independent of the fractal dimension. The calculations have been carried out for $\sigma/E^* = 0.0075$. $C(q)$ and q are measured in m^3 and m^{-1}, respectively.

the rapid increase of the average square slope $m_2 = \langle [h'(x)]^2 \rangle = \int \mathrm{d}q q^2 C(q)$ of the profile.

At smaller frequencies a careful observation of Fig. 5 shows, instead, that (except when $H = 1$) the slope of the deformed profile PSD differs from that of the PSD of the rough profile. By following Persson's theory [25, 27] we should expect that, in this frequency range, the power spectrum of the deformed profile follows a power law of the type $C_v(q) \approx q^{-(2+H)}$, which in a log–log diagram should be represented just by a straight line with slope $-(2+H)$. This is necessarily true for the case of rough profiles with Hurst exponent $H = 1$, since in this case we have shown in Fig. 5 that the slope is equal to $-(2H+1) = -3 = -(2+H)$.

However, for fractal dimensions different from $H = 1$ this is not a foregone conclusion. So let us represent in Fig. 6 the quantities $(2+H)^{-1}\log_{10}[C_v(q)]$ as a function of the wavevector q, for the dimensionless applied load $\sigma/E^* = 0.0075$, and for three different values of the Hurst exponent H, i.e., $H = 0.7$, $H = 0.9$ and $H = 1$. If Persson' predictions were correct these curves should run parallel to each other. Figure 6 seems to confirm this type of behavior. The best fits (dashed lines) of $(2+H)^{-1}\log_{10}[C_v(q)]$ in the low range of q-vectors for the three cases considered ($H = 0.7, 0.9, 1$) have slopes approximately close to -1. In the high range of q-vectors, because of adhesion interaction, the numerically calculated curves move away from the dashed lines, i.e., the slope of the PSD of the elastically deformed solid changes for all the fractal dimensions, except, as already noticed, for $H = 1$.

Because of the crucial importance, in many practical applications (e.g., mixed lubrication, lip seals, static seals) the local interfacial separation $t(x) = v(x) - h(x) + s$ between the deformed profile and the underlying rough rigid surface needs to be analysed. In Fig. 7 we show the PSD of the local separation distribution

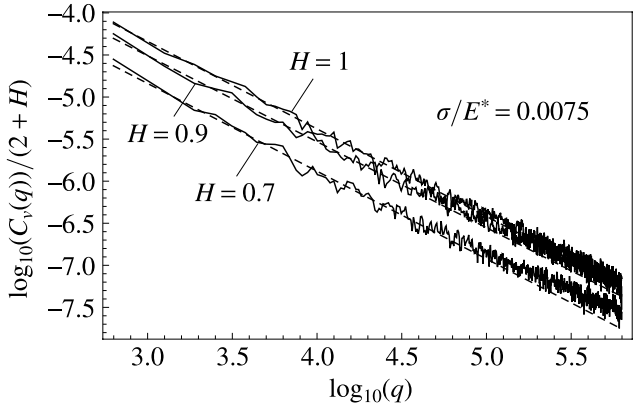

Figure 6. A comparison between the quantities $(2+H)^{-1}\log_{10} C_v(q)$ obtained as a result of the contact between the elastic layer and three different rough surfaces with Hurst exponents $H = 0.7$, $H = 0.9$ and $H = 1$. In the low frequency range the dashed lines (best fits of the numerical data) all have slope close to -1, in agreement with Persson's theory. The calculations have been carried out for $\sigma/E^* = 0.0075$. $C_v(q)$ and q are measured in m^3 and m^{-1}, respectively.

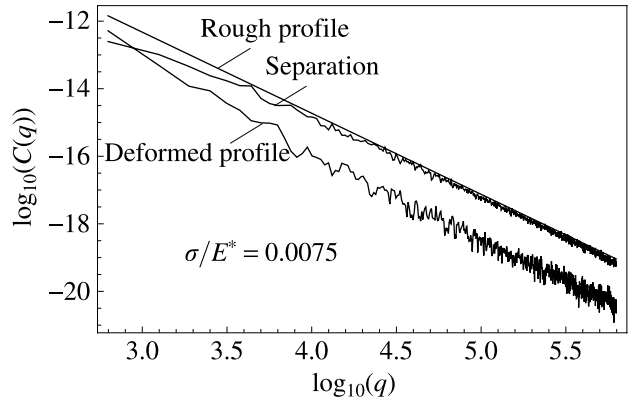

Figure 7. The PSD of the rigid substrate profile for fractal dimension $D_f = 1.3$ compared to the PSD of the deformed shape, and that of the interfacial separation $t(x)$. The curves have been obtained for $\gamma = 0.05$ J/m^2 and $\sigma/E^* = 0.0075$. $C(q)$ and q are measured in m^3 and m^{-1}, respectively.

$t(x)$. As expected, since in the non-contact regions the deformed profile is much smoother than the underlying rough surface, the high frequency spectral content of $t(x)$ must almost be the same as that of the rough surface. Indeed the PSD of the rigid substrate profile and the PSD of the interfacial separation almost perfectly overlap in a wide range of spatial frequencies. This is at least a partial confirmation of the assumptions made in [5, 36] to estimate the root mean square and the probability density function of local separations. Figure 8 shows the normalized probability density function (PDF) $p(t)$ of the interfacial separation $t(x)$ in the non-contact area (where $t > 0$), for $H = 0.7$, and $\gamma = 0.05$ J/m^2. Of course, the probability density function $P(t)$ of $t(x)$ in the nominal contact area differs from

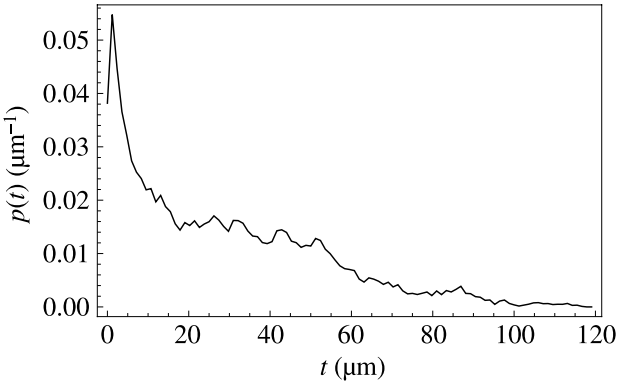

Figure 8. The normalized probability density function (PDF) $p(t)$ of the local separation $t(x)$ in the non-contact area ($t(x) > 0$) for $H = 0.7$ and $\gamma = 0.05$ J/m^2, $\sigma/E^* = 0.011$.

$p(t)$, since it has a delta function at the origin with its weight determined by the area of real contact i.e., given by $A/A_0\delta(t)$, where A is the real contact area and A_0 is the non-contact area; therefore, we can write $P(t) = A/A_0\delta(t) + (1 - A/A_0)p(t)$. Interestingly, the trend of the calculated $p(t)$ appears in good agreement with some theoretical prediction by Persson [36].

Until now our discussion has been focused on the PSDs of deformed profiles and local separations $t(x)$, and on the probability density function of $t(x)$. However, it is also crucial to look at the true contact area and how it depends on fractal dimension D_f. As discussed in Section 1 both multiasperity contact models and Persson's theory predict an asymptotic linearity between the true contact area and the applied mean load through the relation

$$\frac{A}{A_0} = \kappa \frac{\sigma}{E^* m_2^{1/2}} \tag{10}$$

where σ is the external applied load and the predicted values of the factor κ differ depending on which model one employs: multiasperity contact theories or Persson's theory.

Following these theories the fractal dimension D_f of the profile should enter only through the term $m_2^{1/2}$. Thus, two rough profiles with different fractal dimensions but with the same value of m_2 should also present the same contact area *vs*. load relation. In particular Persson's theory shows that even out of the linear range, D_f should not affect directly the contact area *vs*. load relation. In order to verify this theoretical prediction in Fig. 9 the quantity A/A_0 obtained from our numerical calculations is shown, for different values of H, as a function of $\tilde{\sigma}/\sqrt{m_2}$, where $\tilde{\sigma} = 2\sigma/(E^* q_0 h_{\max})$. One can observe that for small loads, as predicted by the theories, the true contact area is only marginally affected by the fractal dimension. In particular for $H = 0.7$ and 0.8 the curves almost perfectly overlap. However, when the load is increased the influence of D_f becomes significant, in contrast with the predictions of the existing theories.

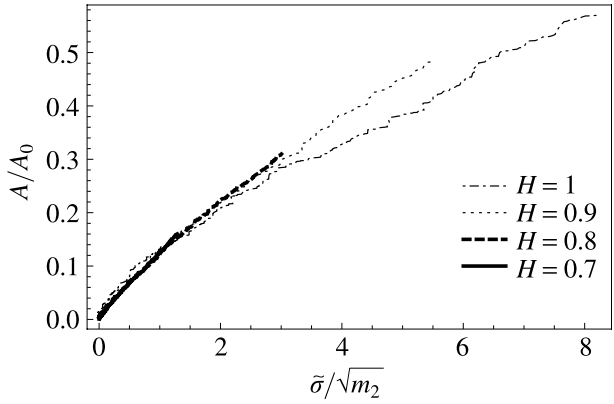

Figure 9. The true contact area A/A_0 as a function of the quantity $\tilde{\sigma}/\sqrt{m_2}$, where $\tilde{\sigma} = 2\sigma/(E^* q_0 h_{\max})$ is the dimensionless applied load, for four different Hurst exponents $H = 0.7$, $H = 0.8$, $H = 0.9$ and $H = 1$. As predicted by the theories, there is only a marginal influence of the fractal dimension on the true contact area at small loads, while for high load values the influence is significant.

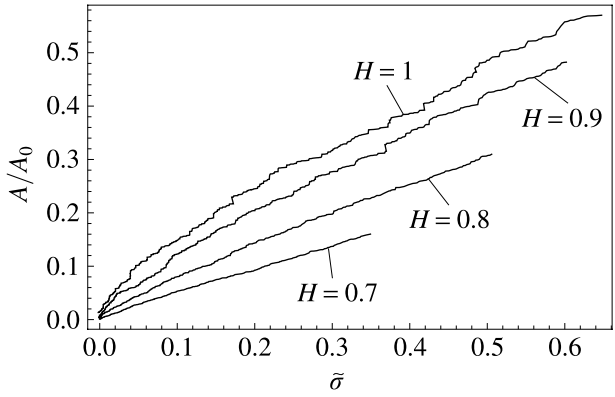

Figure 10. The true contact area A/A_0 as a function of the dimensionless applied load $\tilde{\sigma} = 2\sigma/(E^* q_0 h_{\max})$, for four different Hurst exponents $H = 0.7$, $H = 0.8$, $H = 0.9$ and $H = 1$. Observe that for $H = 1$ (i.e., $D_f = 1$) the curve deviates from linearity.

Interestingly, in Fig. 9 the quantity A/A_0 decreases (given the same value of $\tilde{\sigma}/\sqrt{m_2}$) as the Hurst exponent H is increased. *Vice versa*, in Fig. 10 A/A_0 increases with H, but this time A/A_0 is plotted as a function of $\tilde{\sigma}$. Therefore, it is clear that m_2 plays an important role, and the different behaviours observed in the two aforementioned figures can be explained if one notices that $m_2 = \int_{q_0}^{q_1} \mathrm{d}q q^2 C_R(q) = C_0 q_0^3 [(q_1/q_0)^{2-2H} - 1]/(2 - 2H)$ decreases sufficiently fast as H is increased. It is worth noticing in Fig. 10 that the range of linearity tends to shrink as Hurst's exponent H increases from 0.7 to 1. Moreover the linearity almost disappears when the fractal dimension is $D_f = 1$ (i.e., $H = 1$). This result suggests that the fractal geometry of the rough surface is a key parameter to guar-

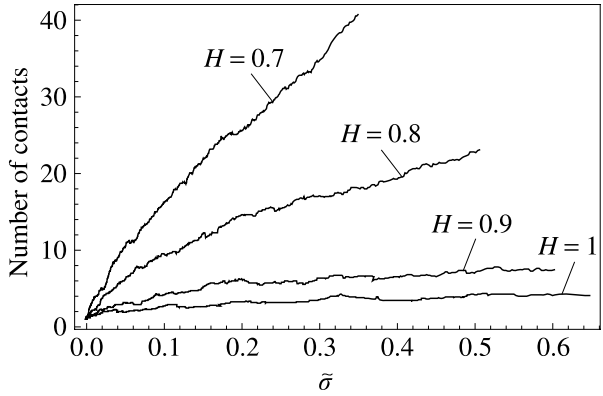

Figure 11. The number of contacts spot as a function of the dimensionless applied load $\tilde{\sigma} = 2\sigma/(E^* q_0 h_{\max})$, for four different Hurst exponents $H = 0.7$, $H = 0.8$, $H = 0.9$ and $H = 1$. Observe that for $H = 0.9$ and $H = 1$ the number of contacts increases very slowly with the load.

antee linearity between contact area and load. The reason is that a sufficiently high fractal dimension makes the contact split in several small contact spots, whose number almost linearly increases with the applied load, whereas the average load in the contact spots remains almost the same. Figure 11 confirms this scenario (see, e.g., the curve at $H = 0.7$) and also shows that for $H = 0.9$ and $H = 1$ the number of contacts changes very slowly as the load is increased. This means that the contact area per single contact spot and the average stress in the contact spot do not remain constant as the load is increased. As a consequence, the contact behavior enters a sort of Hertzian regime, which manifests itself with a lack of linearity between contact area and load.

We now proceed to analyse the influence of the work of adhesion on the PSD of the deformed elastic layer and on the true contact area. In Fig. 12 the PSD of the deformed shape of the elastic body is shown, as resulted from numerical calculations, for $H = 0.7$ and three different values of the work of adhesion $\gamma = 0.03$ J/m^2, $\gamma = 0.04$ J/m^2, $\gamma = 0.05$ J/m^2. The PSD of the rigid substrate profile is also represented. It is clear that in the low-mid range of q-vectors, the PSD of the deformed profiles is not influenced by the work of adhesion. This is expected since at low or mid spatial frequencies the influence of the work of adhesion on the contact behavior is very negligible [18, 35]. At higher frequencies the influence of the work of adhesion is stronger, but still very marginal. In particular, we expect that larger values of the work of adhesion should facilitate full contact conditions to be established in the high q-vectors range, so that the PSD of deformed surface would take slightly larger values as γ is increased. This indeed is what one observes by analysing Fig. 12 in detail. However, the effect of γ is very small and we may conclude that the work of adhesion does not play an important role in determining the PSD of the deformed profile. *Vice versa*, the real contact area is significantly affected by the work of adhesion. Figure 13 shows indeed the values of the true

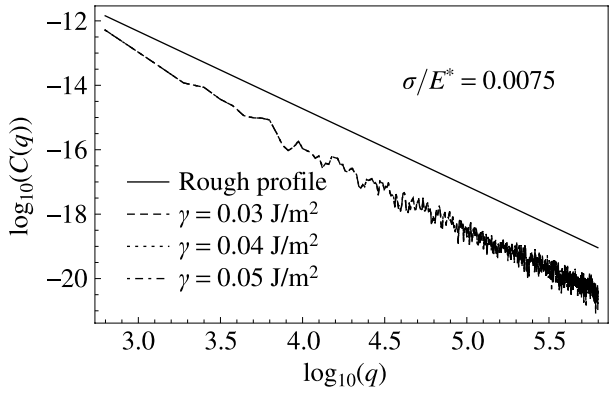

Figure 12. The PSD of the rough profile for $H = 0.7$ compared to the PSD of the deformed shape of the elastic body, obtained from numerical calculations for three different values of the work of adhesion $\gamma = 0.03$ J/m^2, $\gamma = 0.04$ J/m^2, $\gamma = 0.05$ J/m^2. In the low-mid range of q-vectors the PSDs of the deformed profiles are not influenced by the work of adhesion. $C(q)$ and q are measured in m^3 and m^{-1}, respectively.

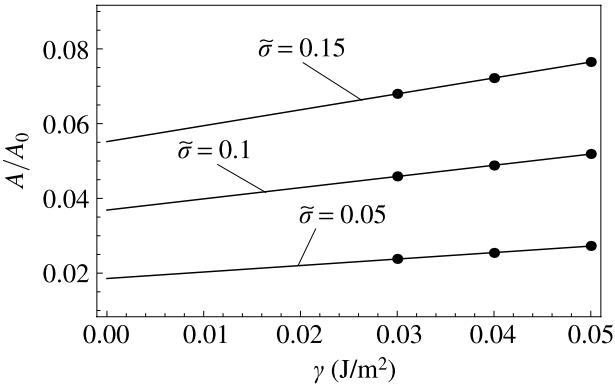

Figure 13. The true contact area A/A_0, for $H = 0.7$, obtained from numerical calculations (points) for three different values of the dimensionless applied load $\tilde{\sigma} = 2\sigma/(E^* q_0 h_{\max})$, $\tilde{\sigma} = 0.05$, $\tilde{\sigma} = 0.1$, $\tilde{\sigma} = 0.15$, and three values of the work of adhesion $\gamma = 0.03$ J/m^2, $\gamma = 0.04$ J/m^2, $\gamma = 0.05$ J/m^2. The solid lines are the linear fits of the data.

contact area A/A_0 (full circles) obtained for three different values of the dimensionless applied load $\tilde{\sigma} = 0.05$, $\tilde{\sigma} = 0.1$, $\tilde{\sigma} = 0.15$, and three different values of the work of adhesion $\gamma = 0.03$ J/m^2, $\gamma = 0.04$ J/m^2 and $\gamma = 0.05$ J/m^2. The solid lines are the linear fits of the data. We observe this time a strong influence of work of adhesion in determining the real contact area and more interestingly a linear relation seems to exist between the true contact area A/A_0 and γ, independently of the applied load. Figure 14 shows the contact area A/A_0 as a function of the dimensionless applied load $\tilde{\sigma}$, for different work of adhesion values $\gamma = 0.03$ J/m^2, $\gamma = 0.04$ J/m^2, $\gamma = 0.05$ J/m^2, the Hurst exponent is $H = 0.7$. Dashed lines represent linear fits of the three curves. The data have also been linearly extrapolated

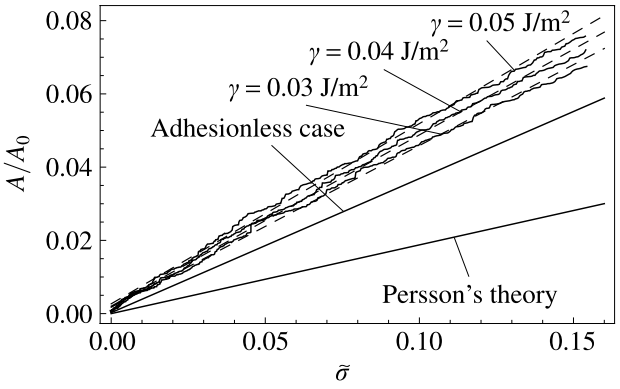

Figure 14. The true contact area A/A_0 as a function of the dimensionless applied load $\tilde{\sigma} = 2\sigma/(E^* q_0 h_{\max})$, for different values of the work of adhesion $\gamma = 0.03$ J/m^2, $\gamma = 0.04$ J/m^2, $\gamma = 0.05$ J/m^2, and for $H = 0.7$. Dashed lines represent the linear fits of the three curves. The data have been linearly extrapolated to the adhesionless case ($\gamma = 0$) by means of the least squares method. Also Persson's predictions for non-adhesion contact is shown.

to the adhesionless case ($\gamma = 0$) by means of the least squares method, and the resulting curve is compared with Persson's predictions for non-adhesion contact. We observe, in agreement with other calculations [25], that, in the linear range, the numerically calculated slope factor $\kappa \approx 3.11$ is almost 2 times the value predicted by Persson's theory, i.e., $\kappa = \sqrt{8/\pi} \approx 1.6$.

4. Conclusion

In this paper the adhesion between a rubber block and a rigid randomly rough profile has been investigated. The roughness has been described by a self-affine fractal, of which the statistical properties are completely determined by the root mean square roughness, its fractal dimension D_f, and by the roll-off and cut-off wavevectors. We have employed a spectral method to generate the randomly rough profiles with different fractal dimensions. For any given D_f and root mean square roughness, several realizations of the same profile (stochastic process) have been generated. The calculated data then have been statistically averaged and the influence of the fractal dimension D_f on the contact area, on the power spectral density of the deformed surface and on the number of contacts in the nominal contact area have been investigated. In particular, we have found that at small load (i.e., in the linear regime between contact area and load) the influence of D_f is negligible. However, at higher load this is no longer true and the influence of the fractal dimension D_f becomes significant. We also found that the linear regime between contact area and load becomes smaller and smaller as the fractal dimension is reduced to a unit value. This result suggests that the fractal geometry of the rough surface is a key parameter to guarantee linearity between contact area and load. Calculations also show that the contact area depends linearly on the work of adhesion, whereas only a negligible

influence of this quantity has been found on the power spectral density (PSD) of the deformed profiles. Moreover, because of its relevance in the field of mixed lubrication and seals, we have calculated the PSD and the probability density function (PDF) of the local separations between the deformed profile and rough rigid surface. We observe that the high-frequency spectral content of the local separation is almost the same as that of the rigid rough surface. This may suggest a methodology to calculate the PDF of the local separation from the existing theories of contact mechanics.

Acknowledgements

This work, as part of the European Science Foundation EUROCORES Programme FANAS, was supported from the EC Sixth Framework Programme, under contract number ERAS-CT-2003-980409. The authors also acknowledge the financial support of Regione Apulia (Italy) within the agreement — Accordo di Programma Quadro in Materia di Ricerca Scientifica — II Atto Integrativo TRASFORMA — code number 28 signed on December 3, 2009.

References

1. B. N. J. Persson and C. Yang, *J. Phys.: Condens. Matter* **20**, 315011 (2008).
2. B. Lorenz and B. N. J. Persson, *European Phys. J. E* **31**, 159–167 (2010).
3. F. Bottiglione, G. Carbone, L. Mangialardi and G. Mantriota, *J. Appl. Phys.* **106**, 104902 (2009).
4. F. Bottiglione, G. Carbone and G. Mantriota, *Tribol. Int.* **42**, 731–737 (2009).
5. M. Scaraggi, G. Carbone, B. N. J. Persson and D. Dini, *Soft Matter* **7**, 10395–10406 (2011).
6. M. Scaraggi, G. Carbone and D. Dini, *Soft Matter* **7**, 10407–10416 (2011).
7. M. Scaraggi and G. Carbone, *J. Mech. Phys. Solids* **58**, 1361–1373 (2010).
8. M. Scaraggi, G. Carbone and D. Dini, *Tribol. Lett.* **43**, 169–174 (2011).
9. B. N. J. Persson, *J. Chem. Phys.* **115**, 3840 (2001).
10. G. Carbone and L. Mangialardi, *J. Mech. Phys. Solids* **52**, 1267–1287 (2004).
11. Y. P. Zhao, L. S. Wang and T. X. Yu, *J. Adhesion Sci. Technol.* **17**, 519–546 (2003).
12. G. Carbone, B. Lorenz, B. N. J. Persson and A. Wohlers, *European Phys. J. E* **29**, 275–284 (2009).
13. J. A. Greenwood and J. B. P. Williamson, *Proc. R. Soc. London A* **295**, 300 (1966).
14. A. W. Bush, R. D. Gibson and T. R. Thomas, *Wear* **35**, 87 (1975).
15. T. R. Thomas, *Rough Surfaces*. Longman Group Limited, New York (1982).
16. J. A. Greenwood, *Wear* **261**, 191–200 (2006).
17. G. Carbone, *J. Mech. Phys. Solids* **57**, 1093–1102 (2009).
18. B. N. J. Persson, *European Phys. J. E* **8**, 385 (2002).
19. B. N. J. Persson, *Surface Sci. Reports* **61**, 201–227 (2006).
20. C. Yang, U. Tartaglino and B. N. J. Persson, *European Phys. J. E* **19**, 47–58 (2006).
21. M. Borri-Brunetto, B. Chiaia and M. Ciavarella, *Comput. Methods Appl. Mech. Eng.* **190**, 6053 (2001).
22. S. Hyun, L. Pei, J.-F. Molinari and M. O. Robbins, *Phys. Rev. E* **70**, 026117 (2004).
23. C. Campañá and M. H. Müser, *Phys. Rev. B* **74**, 075420 (2006).
24. C. Campañá, *Phys. Rev. E* **78**, 026110 (2008).

25. G. Carbone, M. Scaraggi and U. Tartaglino, *European Phys. J. E* **30**, 65–74 (2009).
26. M. Benz, K. J. Rosenberg, E. J. Krame and J. N. Israelachvili, *J. Phys. Chem. B* **110**, 11884–11893 (2006).
27. B. N. J. Persson, *J. Phys.: Condens. Matter* **20**, 312001 (2008).
28. G. Carbone and F. Bottiglione, *J. Mech. Phys. Solids* **56**, 2555–2572 (2008).
29. K. N. G. Fuller and D. Tabor, *Proc. R. Soc. A* **345**, 327–342 (1975).
30. L. X. Zhang and Y. P. Zhao, *J. Adhesion Sci. Technol.* **18**, 715–729 (2004).
31. L. Pei, S. Hyun, J. F. Molinari and M. O. Robbins, *J. Mech. Phys. Solids* **53**, 2385 (2005).
32. G. Carbone, B. Lorenz, B. N. J. Persson and A. Wohlers, *European Phys. J. E* **29**, 275–284 (2009).
33. G. Carbone, M. Scaraggi and C. Putignano, submitted.
34. G. Carbone and L. Mangialardi, *J. Mech. Phys. Solids* **56**, 684–706 (2008).
35. G. Carbone, L. Mangialardi and B. N. J. Persson, *Phys. Rev. B* **70**, 125407 (2004).
36. A. Almqvista, C. Campañá, N. Prodanovb and B. N. J. Persson, *J. Mech. Phys. Solids* **59**, 2355 (2011).